Supplementary Information

Consequence of doping mediated Oxygen vacancies on charge transfer ability of Zinc Oxide Nanosheets for electrochemical glucose sensing

Saptaka Baruah[a], Bidyarani Maibam[a], Jyoti Jaiswal[a], Ankit Kumar[b], and Sanjeev Kumar[a]*
[a]*Centre for Advanced Research, Department of Physics, Rajiv Gandhi University, Arunachal Pradesh-791112, India.*
[b]*Department of Mechanical & Industrial Engineering (MIED), IIT Roorkee, Roorkee 247667, India.*
*Corresponding author email: sanjeev.kumar@rgu.ac.in

S1. Experimental details

S1.1 Synthesis of pristine-ZnO and Ag-doped ZnO nanosheets

In this work, pristine-ZnO, 1% Ag-doped ZnO (ZnO:Ag1), 2% Ag-doped ZnO (ZnO:Ag2), 3% Ag-doped ZnO (ZnO:Ag3), 4% Ag-doped ZnO (ZnO:Ag4) and 5% Ag-doped ZnO (ZnO:Ag5) were synthesized using hydrothermal method. To prepare these samples, firstly, 1 M $Zn(NO_3)_2 .6H_2O$ and 1 M $AgNO_3$ solutions were made in double-distilled water and mixed in proportionality as required. After that 5 M NaOH solution was added dropwise. The mixed solution was stirred continuously for 2 hours and then placed in a Teflon-lined stainless-steel autoclave and kept at 180 °C for 24 hours. The product was then rinsed with double-distilled water and dried for 24 hours at 100 °C before being calcined for 2 hours at 500 °C.

S1.2 Fabrication of ZnO/ITO and Ag-doped ZnO/ITO Electrodes

Indium Tin Oxide (ITO) coated glasses were used as a substrate material for the fabrication of working electrodes. At first, ITO substrates were dipped in ethanol and cleaned by a sonication process followed by thorough rinsing using double-distilled water. Now, for the fabrication of the ZnO/ITO electrode, 10 µL solution of dispersed ZnO nanosheets was drop-casted onto ITO-coated glass. Likewise, 1% to 5% of Ag-doped ZnO electrodes were fabricated using the same process. Finally, the prepared electrodes were dried at room temperature for 24 hours.

S1.3 Immobilization of GO_x on the electrodes

For the application of enzymatic glucose sensing, prior to immobilization, freshly prepared GO_x solution (10 µL, 4 mg/mL) was dropped on the ZnO/ITO, ZnO:Ag2/ITO, and ZnO:Ag5/ITO electrodes, and then the electrodes were dried at room temperature for 30 min. To eliminate mobilized GO_x, the electrodes were rinsed with distilled water. Since the enzyme denatures when exposed to ambient temperature for an extended period, the immobilized electrode was stored at 4 °C when not in use.

S2. Results and discussion

S2.1 Characterization of synthesized pristine and Ag-doped ZnO nanosheets

Figure 2 shows the FESEM micrograph of the pristine and Ag-doped ZnO samples at low and high resolution (corresponding inset Figure 2). FESEM images (Figure 2(a-d)) revealed the development of nanosheets in pristine-ZnO, ZnO:Ag1, ZnO:Ag2, and ZnO:Ag3. While the mixture of nanosheets and dendrite-like structures were found in ZnO:Ag4 and ZnO:Ag5 (Figure 2(e,f)). Doping may cause the asymmetrical and multidimensional growth in ZnO:Ag4 and ZnO:Ag5 which result in the formation of dendrite-like structures [2]. The size and thickness of pristine-ZnO and Ag-doped ZnO nanosheets were found to decrease with an increase in dopant concentration. This is because metal-doping in ZnO at an appropriate level inhibits particle growth due to the symmetry-breaking effects of the dopant at the grain boundary [3, 4].

As shown in Figure S1(a), for pristine-ZnO, the EDX spectra revealed 47.80 at% of O, 52.20 at% of Zn. While spectra of ZnO:Ag5 (Figure S1(b)) revealed 44.82 at% of O and 52.46 at% of Zn and 2.72 at% of Ag with 6.61 wt%. EDX results further confirm the formation of pristine-ZnO and the successful incorporation of Ag dopants in the ZnO host matrix.

Figure S3 shows the FTIR spectra for the pristine-ZnO, GOx/ZnO, ZnO:Ag2, GOx/ZnO:Ag2, ZnO:Ag5, and GOx/ZnO:Ag5 samples. FTIR spectra of pristine-ZnO revealed the multiple bands observed at ~3439.18 cm^{-1} (O-H stretching), ~1633.54 and ~1384 cm^{-1} (H-O-H bending vibration), ~1029.78 cm^{-1} (O-H bending mode), and ~557.68 and ~465 cm^{-1} (stretching vibration of Zn-O) indicating the formation of ZnO including the presence of small quantity of moisture and hydroxyl group on the surface of ZnO [5-7]. However, for ZnO:Ag2 and ZnO:Ag5, a small shift towards the low frequencies was noted, which indicates the successful incorporation of Ag ions into the ZnO matrix [8]. The reduction in band intensity observed in Ag-doped ZnO may be due to the formation of Ag particles on the surface of pristine-ZnO [9, 10], which is also corroborated with our XRD results. Further, FTIR spectra of GOx/ZnO matrix demonstrated absorption bands at ~3455.17 cm^{-1} (combination of both N-H and O-H stretching), ~2352.97 cm^{-1} (N-H stretching vibration), ~1072.64 cm^{-1} (phosphate ion adsorption), ~536.61 cm^{-1} (stretching vibration of Zn-O), and three bands linked to the peptide structure, i.e., amide I ~1645.76 cm^{-1} (C=O stretching and H-O-H bending vibration), amide II ~1551 cm^{-1} (N-H bending) and amide III ~1241.3 (C-N and C-H stretching), which confirm the successful immobilization of GOx on the pristine-ZnO matrix [11, 12]. However, the same characteristic bands for GOx were also observed for GOx/ZnO:Ag2 and GOx/ZnO:Ag5 samples, signifying further the successful immobilization of GOx on the surface of the Ag-doped ZnO samples.

References

[1] Ridhuan, N. S., Razak, K. A., & Lockman, Z. (2018). Fabrication and characterization of glucose biosensors by using hydrothermally grown ZnO nanorods. *Scientific reports*, *8*(1), 1-12.

[2] Maibam, B., Baruah, S., & Kumar, S. (2020). Photoluminescence and intrinsic ferromagnetism of Fe doped zinc oxide. *SN Applied Sciences*, *2*(10), 1-11.

[3] Khan, M. M., Kumar, S., Khan, M. N., Ahamed, M., & Al Dwayyan, A. S. (2014). Microstructure and blueshift in optical band gap of nanocrystalline AlxZn1− xO thin films. *Journal of luminescence*, *155*, 275-281.

[4] Ahamed, M., Khan, M. A., Akhtar, M. J., Alhadlaq, H. A., & Alshamsan, A. (2017). Ag-doping regulates the cytotoxicity of TiO2 nanoparticles via oxidative stress in human cancer cells. *Scientific reports*, *7*(1), 1-14.

[5] Goswami, M., Adhikary, N. C., & Bhattacharjee, S. (2018). Effect of annealing temperatures on the structural and optical properties of zinc oxide nanoparticles prepared by chemical precipitation method. *Optik*, *158*, 1006-1015.

[6] Raja, K., Ramesh, P. S., & Geetha, D. (2014). Structural, FTIR and photoluminescence studies of Fe doped ZnO nanopowder by co-precipitation method. *Spectrochimica Acta Part A: Molecular and Biomolecular Spectroscopy*, *131*, 183-188.

[7] Reddy, A. J., Kokila, M. K., Nagabhushana, H., Chakradhar, R. P. S., Shivakumara, C., Rao, J. L., & Nagabhushana, B. M. (2011). Structural, optical and EPR studies on ZnO: Cu nanopowders prepared via low temperature solution combustion synthesis. *Journal of Alloys and Compounds*, *509*(17), 5349-5355.

[8] Wannes, H. B., Dimassi, W. R., Zaghouani, B., & Mendes, M. J. (2017). Li-doped ZnO Sol-Gel Thin Films: Correlation between Structural Morphological and Optical Properties. *J Textile Sci Eng*, *8*(328), 2.

[9] Nagaraju, G., Prashanth, S. A., Shastri, M., Yathish, K. V., Anupama, C., & Rangappa, D. (2017). Electrochemical heavy metal detection, photocatalytic, photoluminescence, biodiesel production and antibacterial activities of Ag–ZnO nanomaterial. *Materials Research Bulletin*, *94*, 54-63.

[10] Zamiri, R., Rebelo, A., Zamiri, G., Adnani, A., Kuashal, A., Belsley, M. S., & Ferreira, J. M. F. (2014). Far-infrared optical constants of ZnO and ZnO/Ag nanostructures. *RSC Advances*, *4*(40), 20902-20908.

[11] Singh, P., Benjakul, S., Maqsood, S., & Kishimura, H. (2011). Isolation and characterisation of collagen extracted from the skin of striped catfish (Pangasianodon hypophthalmus). *Food chemistry*, *124*(1), 97-105.

[12] Uc-Cayetano, E. G., Ordóñez, L. C., Cauich-Rodríguez, J. V., & Avilés, F. (2016). Enhancement of electrochemical glucose sensing by using multiwall carbon nanotubes decorated with iron oxide nanoparticles. *Int. J. Electrochem. Sci*, *11*, 6356-6369.

Table

Table S1: Binding energy values of $Zn2p_{3/2}$, $Zn2p_{1/2}$, O1s, and the ratio of the sub-peaks area $\frac{O(II)}{O(I)+O(II)}$ for the pristine and Ag-doped ZnO nanosheets.

Sample	Binding energy (eV)							Ratio of sub-peaks area $O(II)/[O(I)+O(II)]$
	Zn2p		O1s			Ag3d		
	$Zn2p_{3/2}$	$Zn2p_{1/2}$	O(I)	O(II)	O(III)	$Ag3d_{5/2}$	$Ag3d_{3/2}$	
ZnO	~1021.15	~1044.15	~529.97	~531.24	~531.9	—	—	~0.9
ZnO:Ag5	~1020.92	~1043.92	~529.61	~530.71	~532.7	~368.81	~374.81	~0.4

Table S2: EIS parameters obtained by fitting the Nyquist plot with the equivalent circuit for the pristine and Ag-doped ZnO nanosheets based electrodes.

Sample	$C_{dl} \times 10^{-6}$ (F)	R_s (Ω)	R_{ct} (Ω)	$Z_w \times 10^{-2}$ ($Ss^{1/2}$)
ZnO/ITO	~6.1	~83.2	~148.4	~1.2
ZnO:Ag1/ITO	~2.9	~130.2	~131.8	~0.7
ZnO:Ag2/ITO	~8.9	~77.7	~114	~1.4
ZnO:Ag3/ITO	~6.6	~99.9	~101.6	~1.3
ZnO:Ag4/ITO	~5.3	~120	~82.6	~1.31
ZnO:Ag5/ITO	~10.2	~78.5	~51.9	~2.33

Table S3: The $\frac{I_{pa}}{I_{pc}}$ ratio at scan rate 10 mV/s, diffusion coefficient (D), surface concentration (I^*), electroactive surface area (A_e), sensitivity, Michaelis-Menten constant (K_m^{app}), limit of detection (LOD) and linear range of prepared electrodes.

Samples	I_{pa}/I_{pc}	$D \times 10^{-6}$ ($cm^2\ s^{-1}$)	$I^* \times 10^{-9}$ (mol cm^{-2})	A_e (cm^2)	Sensitivity ($\mu AMm^{-1}cm^{-2}$)	K_m^{app} (mM)	LOD (mM)	Linear range (mM)
ZnO/ITO	1.03	3.62	5.75	0.68	—	—	—	—
ZnO:Ag1/ITO	1.04	6.19	7.58	0.682	—	—	—	—
ZnO:Ag2/ITO	1.02	6.82	8.33	0.713	—	—	—	—
ZnO:Ag3/ITO	1.02	9.86	9.61	0.685	—	—	—	—
ZnO:Ag4/ITO	1.03	13.9	11.4	0.686	—	—	—	—
ZnO:Ag5/ITO	1.1	16.2	13.7	0.746	104.7	—	0.06	0-4
GOx/ZnO/ITO	1.05	3.29	4.97	0.618	37.5	0.07	0.204	0-3
GOx/ZnO:Ag2/ITO	1.02	4.32	6.30	0.683	15.3	0.04	0.451	0-3
GOx/ZnO:Ag5/ITO	1.05	6.12	5.38	0.487	98.3	0.26	0.098	0-3

Figures

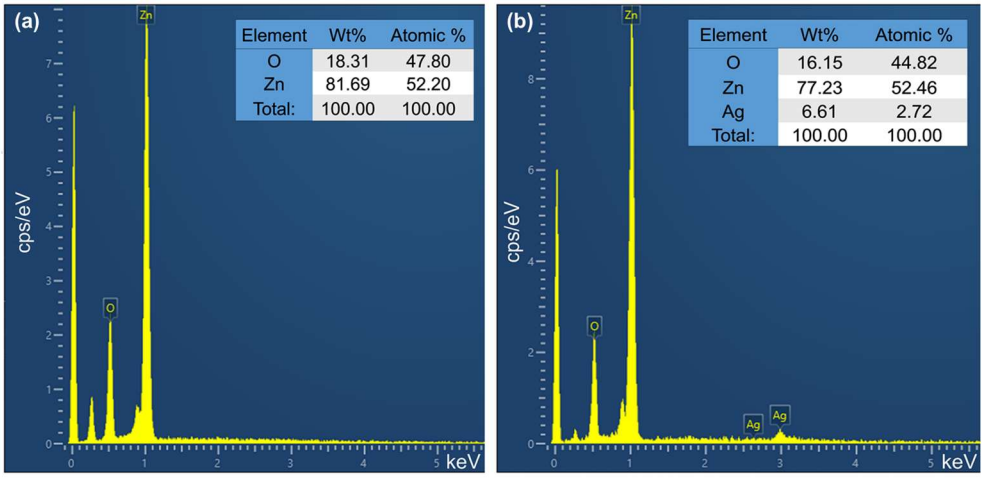

Figure S1: EDX spectra of (a) pristine-ZnO and (b) ZnO:Ag5 nanosheets.

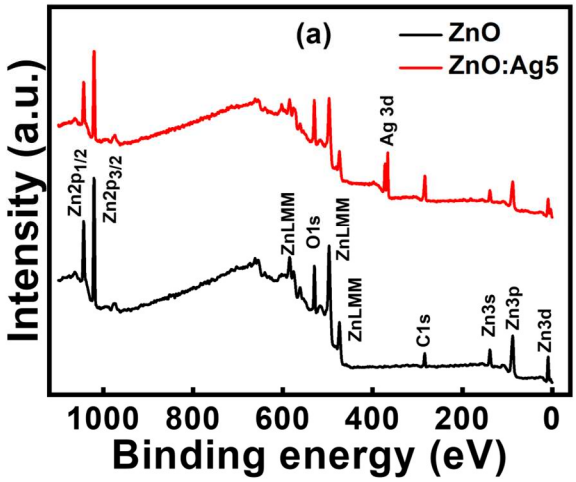

Figure S2: The XPS survey scan of the pristine-ZnO and ZnO:Ag5 nanosheets.

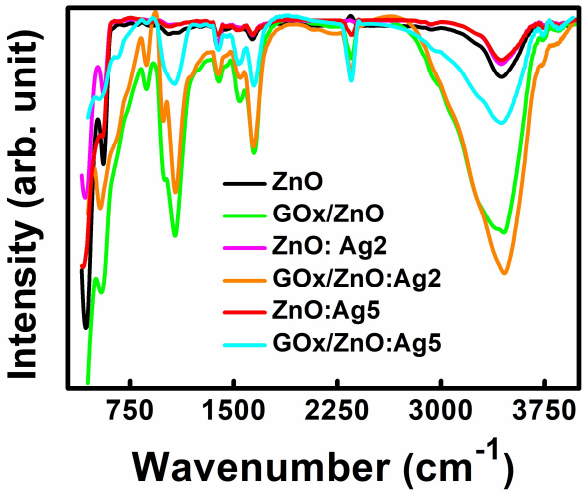

Figure S3: FTIR spectra for pristine-ZnO, GOx/ZnO, ZnO:Ag2, GOx/ZnO:Ag2, ZnO:Ag5, and GOx/ZnO:Ag5 samples.

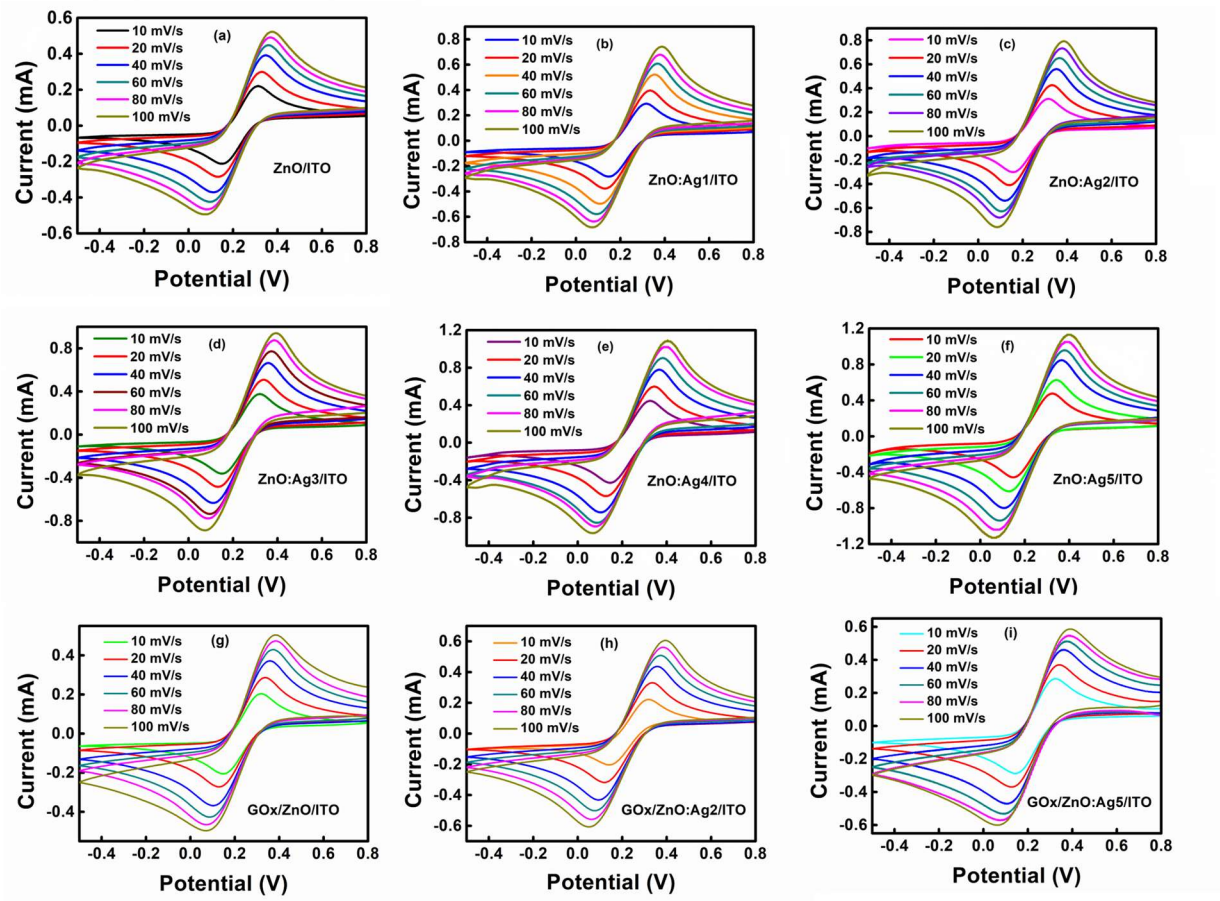

Figure S4: Cyclic voltammogram (CV) of all the prepared electrodes: (a) ZnO/ITO, (b) ZnO:Ag1/ITO, (c) ZnO:Ag2/ITO, (d) ZnO:Ag3/ITO, (e) ZnO:Ag4/ITO, (f) ZnO:Ag5/ITO, (g) GOx/ZnO/ITO, (h) GOx/ZnO:Ag2/ITO, and (i) GOx/ZnO:Ag5/ITO in 0.01 M PBS (pH 7.4) buffer solution containing 5 mM $[Fe(CN)_6]^{3-/4-}$ at different scan rates within 10-100 mV s^{-1}.

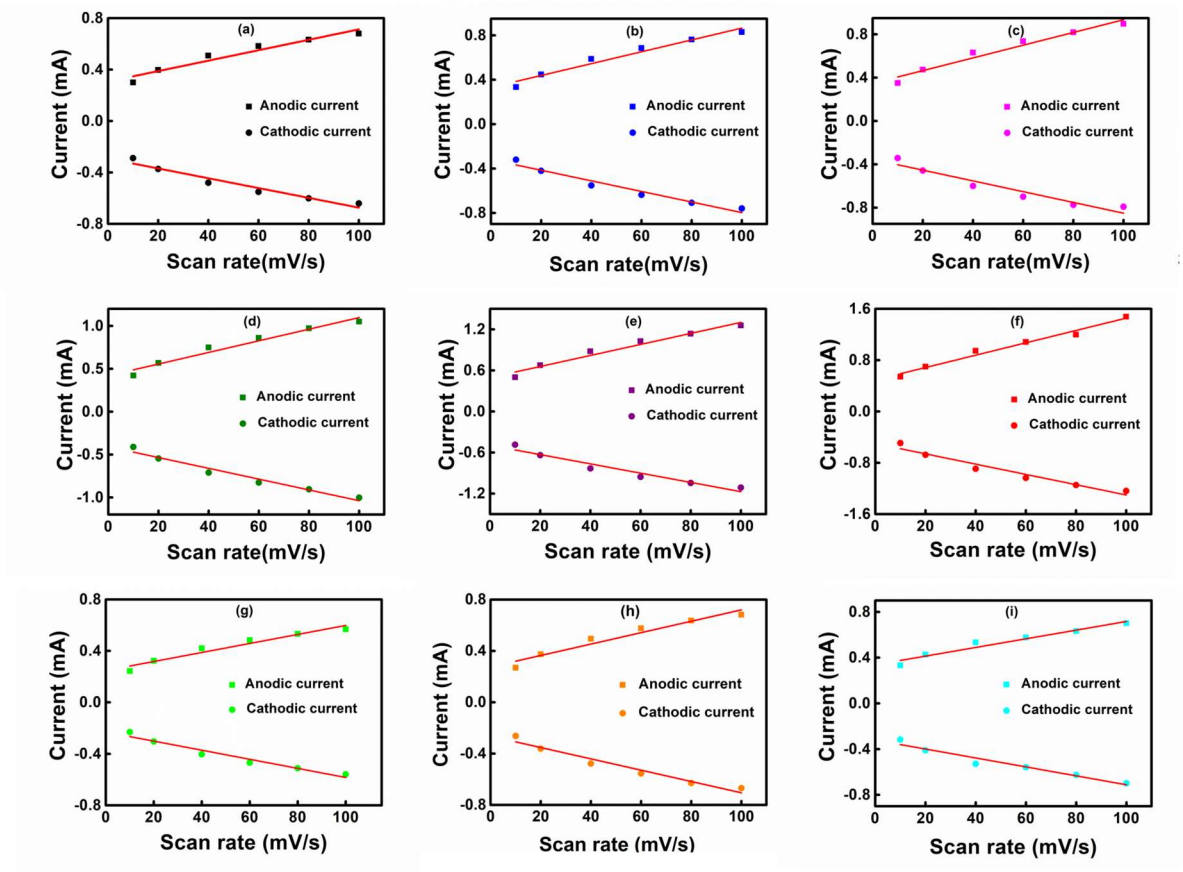

Figure S5: Peak current vs scan rate of all the prepared electrodes: (a) ZnO/ITO, (b) ZnO:Ag1/ITO, (c) ZnO:Ag2/ITO, (d) ZnO:Ag3/ITO, (e) ZnO:Ag4/ITO, (f) ZnO:Ag5/ITO, (g) GOx/ZnO/ITO, (h) GOx/ZnO:Ag2/ITO, and (i) GOx/ZnO:Ag5/ITO.

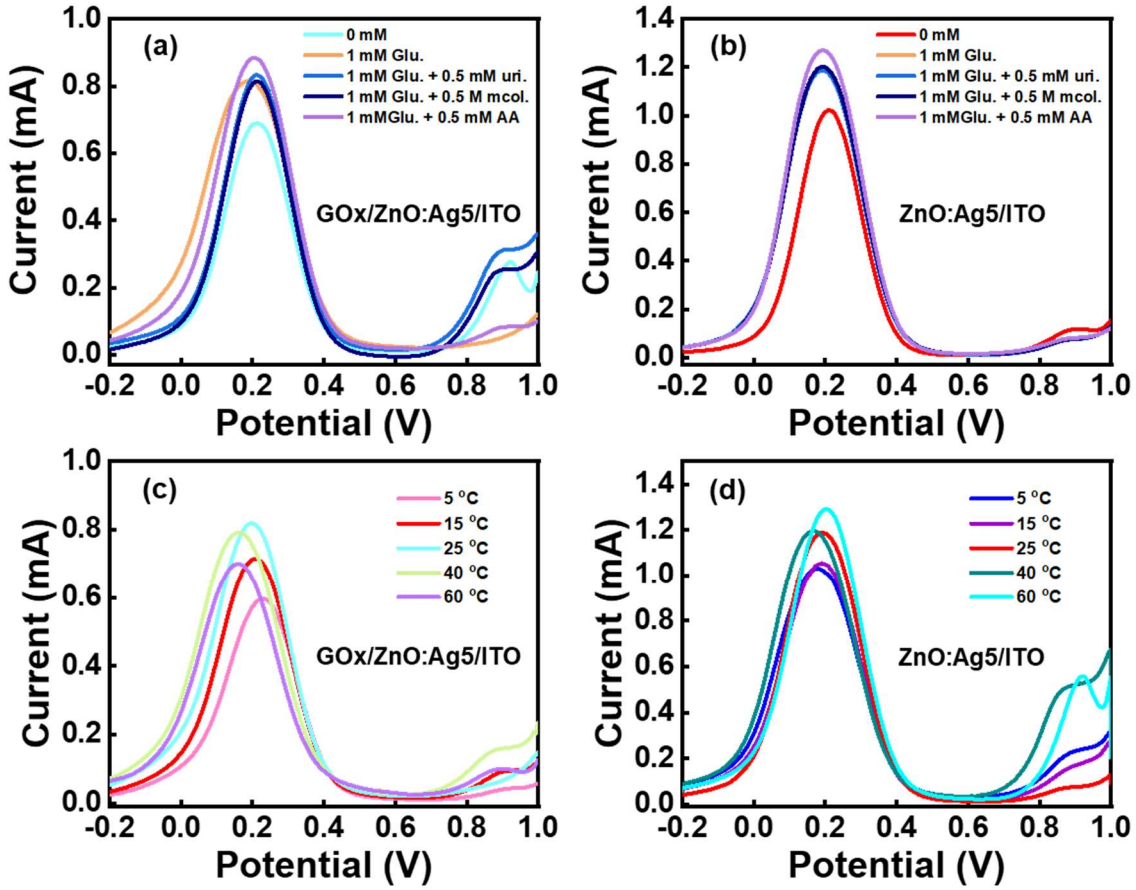

Figure S6: Square wave voltammogram (SWV) of the (a) GOx/ZnO:Ag5/ITO and (b) ZnO:Ag5/ITO electrodes in the presence of 1 mM glucose with 0.5 mM interfering species (Cholesterol, Uric Acid (UA) and Ascorbic Acid (AA)) in 0.01 M PBS (pH 7.4) buffer solution containing 5 mM $[Fe(CN)_6]^{3-/4-}$. SWV of the (c) GOx/ZnO:Ag5/ITO and (d) ZnO:Ag5/ITO electrodes at different temperatures (5-60 °C) in 0.01 M PBS (pH 7.4) buffer solution containing 5 mM $[Fe(CN)_6]^{3-/4-}$ and 1 mM glucose.

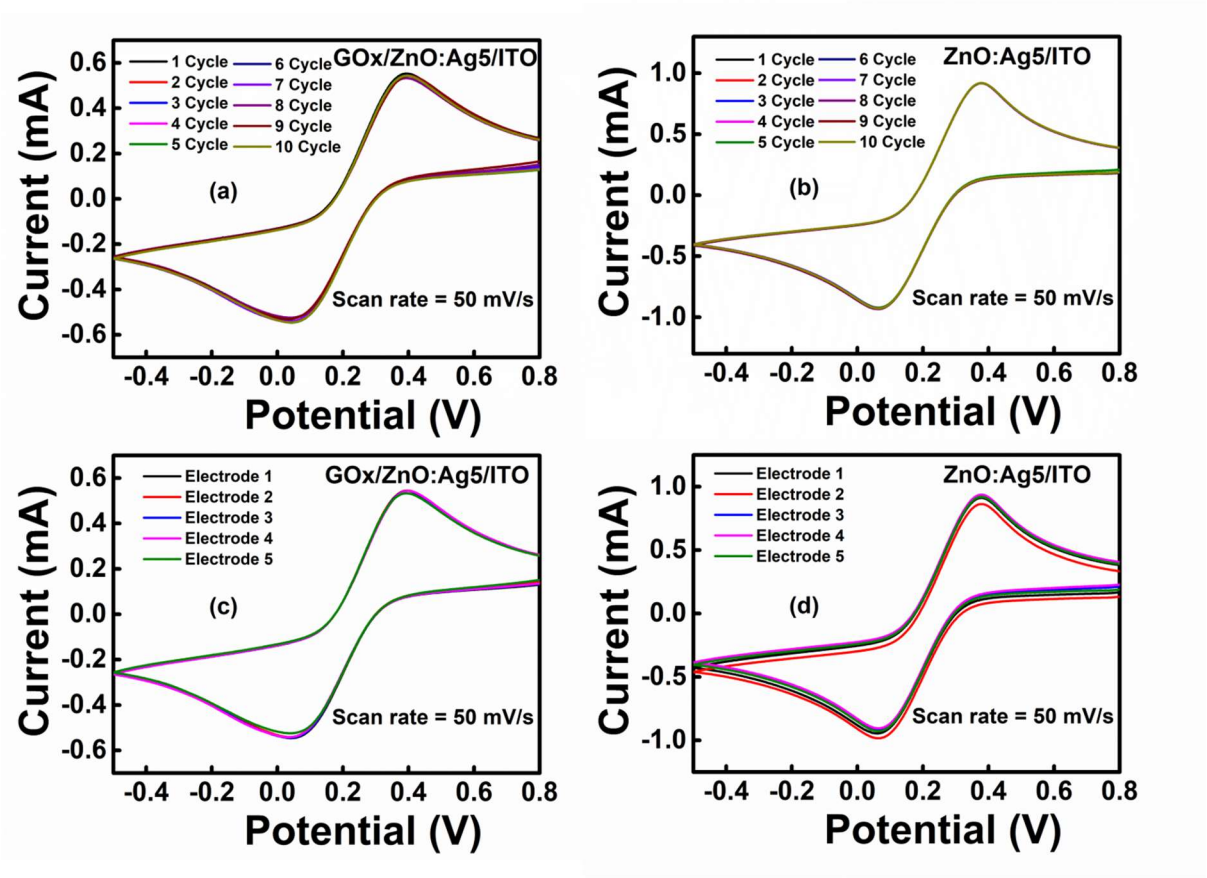

Figure S7: CV of the GOx/ZnO:Ag5/ITO (a) and ZnO:Ag5/ITO (b) electrodes with 10 measurements at scan rate of 50 mV s^{-1} in 0.01 M PBS (pH 7.4) buffer solution containing 5 mM $[Fe(CN)_6]^{3-/4-}$ and 1 mM glucose. CV of five different GOx/ZnO:Ag5/ITO (c) and ZnO:Ag5/ITO (d) electrodes at scan rate of 50 mV s^{-1} in 0.01 M PBS (pH 7.4) buffer solution containing 5 mM $[Fe(CN)_6]^{3-/4-}$ and 1 mM glucose.